Renewable Energy 116 (2018) 335–343

Contents lists available at ScienceDirect

Renewable Energy

journal homepage: www.elsevier.com/locate/renene

The solar noise barrier project: 3. The effects of seasonal spectral variation, cloud cover and heat distribution on the performance of full-scale luminescent solar concentrator panels

Michael G. Debije [a, *], Chris Tzikas [b], Minne M. de Jong [b], Michalis Kanellis [c], Lenneke H. Slooff [d]

[a] Dept. Chemical Engineering & Chemistry, Eindhoven University of Technology, 5600 MB, Eindhoven, The Netherlands
[b] Solar Energy Application Centre, 5656 AE, Eindhoven, The Netherlands
[c] Smart Energy Buildings & Cities, Eindhoven University of Technology, 5600 MB, Eindhoven, The Netherlands
[d] Energy Research Centre of the Netherlands (ECN), 1755 ZG, Petten, The Netherlands

ARTICLE INFO

Article history:
Received 6 April 2017
Received in revised form
15 August 2017
Accepted 22 September 2017
Available online 28 September 2017

Keywords:
Luminescent solar concentrator
Photovoltaics
Temperature
Indirect light
Spectra

ABSTRACT

We report on the relative performances of two large-scale luminescent solar concentrator (LSC) noise barriers placed in an outdoor environment monitored for over a year. Comparisons are made for the performances of a number of attached photovoltaic cells with changing spectral illumination, cloud cover conditions and other seasonal variations, and the temperatures of the cells. Differences in performance are attributed to the positioning of the panels, whether facing North/South or East/West. In general, the panels facing East/West run cooler than those facing North/South. The LSCs in both orientations appear to perform more efficiently under lower light conditions: one factor contributing to this increased performance is better spectral matching of the solar spectrum under cloudy conditions to the absorption spectrum of the embedded fluorescent dye. This work is a step forward in the characterization of a large-scale LSC device, and suggests predictions of performance of devices could be made for any location given sufficient knowledge of the illumination conditions, and provides an important step towards the commercialization of these alternative solar energy generators for the urban setting.

1. Introduction

The luminescent solar concentrator (LSC) is a device with the potential of bringing attractive solar energy generating devices into an urban center [1]. First described in the late 1970's [2,3], the LSC has mainly been confined to the laboratory, with only a few examples of full-scale devices being deployed for research purposes [4–8]. The LSC is based on the concept of using a luminophore embedded in a large-area polymer plate. The luminophore absorbs a fraction of the incident sunlight: because of the nature of the luminophore absorption, both direct and indirect sunlight can be equally absorbed [9]. The absorbed light is then emitted by the luminophore. Since the plastic plate has a higher refractive index than the surrounding air, it will act as a lightguide, trapping a significant fraction of the emitted light within the polymer. The guided light can then only escape through the edges, where photovoltaic (PV) cells can be placed to convert the emission light into electricity [10–12].

For the LSC to attain commercial success, it is necessary they be tested in real-world environments, at realistic sizes. With this in mind, we constructed two large scale LSC-based panels in a noise barrier configuration and installed them outdoors alongside a major roadway in the Netherlands and monitored their performance for a little over one year. We have previously reported on several aspects of the LSC noise barrier (the SONOB project) performance. In our first work, we focused on the effect of variation in solar position with respect to the surface plane of the barrier for both North/South and East/West facing barrier panels, and noted the self-shading seen by the frame of the device as we tracked performance during the span of a single day [13]. The second work considered the effect of application of graffiti and street art on the surface of the barrier, and the impact it had on performance of the individual cell strips attached to the edges of the device [14].

In this work, we consider the seasonal changes, the effects of

* Corresponding author.
E-mail address: m.g.debije@tue.nl (M.G. Debije).

https://doi.org/10.1016/j.renene.2017.09.079

external temperature, and the effect of cloud cover on the general performance of the LSC barriers. We show the relative performance of the device tracks well with the variations of the seasonal solar spectrum, suggesting output of the LSC can be predicted if local solar conditions are known. The PV cells attached to the edges of the LSC plates demonstrate temperature increases with respect to the ambient conditions, but this may be dramatically affected by the orientation of the panels: East/West barriers show quite a different response than North/South facing barriers. Finally, the response of the LSC is relatively insensitive to the cloud condition, similar to what was seen in scale model devices.

2. Experimental

Two cast PMMA plates $1 \times 5 \times 0.012$ m^3 were used in the large-scale experimental setup. One contained the fluorescent dye Lumogen Red305 [15] and one contained the fluorescent dye Lumogen Orange240 (both dyes purchased from BASF). The top and bottom Red305 panel edges were attached with two strips of series connected monocrystalline silicon PV cells or GaAs cells. Fig. 1a below shows the positioning of the cell strips on the Red305 LSC plates. The strip pairs of series connected monocrystalline silicon PV cells each contained seven 12×78 mm^2 cells, and were mounted at four different locations on the LSC plate, labelled TS (Top, Side), TM (Top, Middle), BM (Bottom, Middle) and BS (Bottom, Side) by a silicone-based, optically transparent flexible glue. The GaAs cell strips were mounted in a similar fashion at the locations indicated in Fig. 1a. On the Orange240 LSC plate, only 2 strings of two cell strips were placed in the middle right position, each strip containing seven 12×78 mm^2 cells. White tape masked the overhang to the edge of the LSC lightguide plate. The performance of each of the cell strip pairs was independently monitored. The vertical edges of each LSC panel were affixed with a white scatterer.

Two noise barrier assemblies were created, overseen by Van Campen Industries. Each consisted of four panels: a Red305 panel was on top, the Orange240 below this, and the two bottom panels hosting mounted silicon bi- and mono-facial PVs, as may be seen in Fig. 1b. Heijmans installed the two assembled noise barriers with one barrier facing North/South and the other East/West in the city of Den Bosch, the Netherlands. The tilts were such that the barriers reclined 15° towards the North and East, respectively. The barriers' wiring was attached by SEAC to the various detectors used in the experiments and the controlling computer. Two EKO MS-802 pyrometers were mounted atop both the barriers, in plane with the front and rear side of the barrier to collect information on irradiance. The output of the PV cells was monitored by an EKO MP-160 IV tracer in combination with a number of switching units.

3. Results and discussion

3.1. Effect of the seasonal spectral fluctuations

It is already known that the spectral distribution of sunlight changes over the course of a day and over the period of a year [16]. Previously, we demonstrated LSC performance varied in response to changes in spectral quality [9]. In general, increased cloud cover shifts the effective spectra towards the blue owing to the rejection of infrared light [17]. In general, this is a positive feature for LSCs, especially those based on organic luminophores, which tend to be most effective at absorbing shorter wavelengths of light. The overall efficiency of the LSC increases with cloudy conditions (of course, absolute output drops due to reduced intensity incident on the lightguide). Still, this increased performance efficiency under low light and blue-shifted spectra is in direct contrast to the performance of silicon-based PV, which in general perform less well in low light and reduced efficiency in blue-shifted spectra [18,19].

Fig. 2 shows a monthly-averaged spectrum of the incident solar light measured at the barrier site at 13:00 for a whole measurement year. The Red305 dye absorbs only part of the solar spectrum (see Fig. 3): a shift in the solar spectrum can cause changes in the collected current by the cells [9].

To compare performance in the LSC noise barriers, we use the 'performance ratio', *PR*, for the attached cells. The definition of PR is [13].

$$PR = \frac{Field\ Efficiency}{Theoretical\ Efficiency} = \frac{P_{measured}(W)}{P_{rated}(W)} \times \frac{E_{stc}\left(W/m^2\right)}{E_{measured}\left(W/m^2\right)} \quad (1)$$

where $E_{stc} = 1000$ W/m^2, P_{rated} is the nominal power outputs of the cell, $P_{measured}$ is determined from the maximum power point on the PV cell I-V curve, and the total measured irradiance from both sides of the LSC panel at the test site is $E_{measured}$. The PVs used had fill factors around 80%. As described earlier [13], PR may not be an ideal parameter to describe LSC performance, but gives a comparison between cell performances given similar weather and lighting conditions. Since the data presented in this paper is based on single large LSC panels, less emphasis should be placed on comparing absolute numbers of PV cell strips but more on the relative performance of individual cell strips throughout a measurement period: there are variations between the strips arising from differences in the optical connection between the polymer plate and the cell strips.

The PR is determined by comparing the performance outdoors

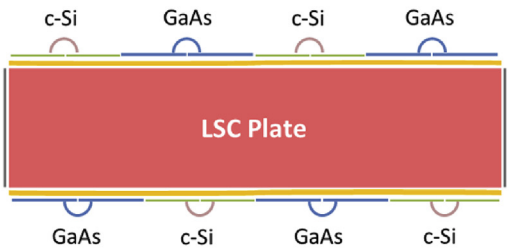

Fig. 1. a) Positioning of the cell strips along the Red305 LSC plates as seen from the side facing the road. Around the Orange240 plates, only two c-Si and two GaAs strips were placed, in the middle-right position. b) Photograph of the LSC noise barrier site. The barrier to the left in the image faces North/South, and the right barrier in the image faces East/West.

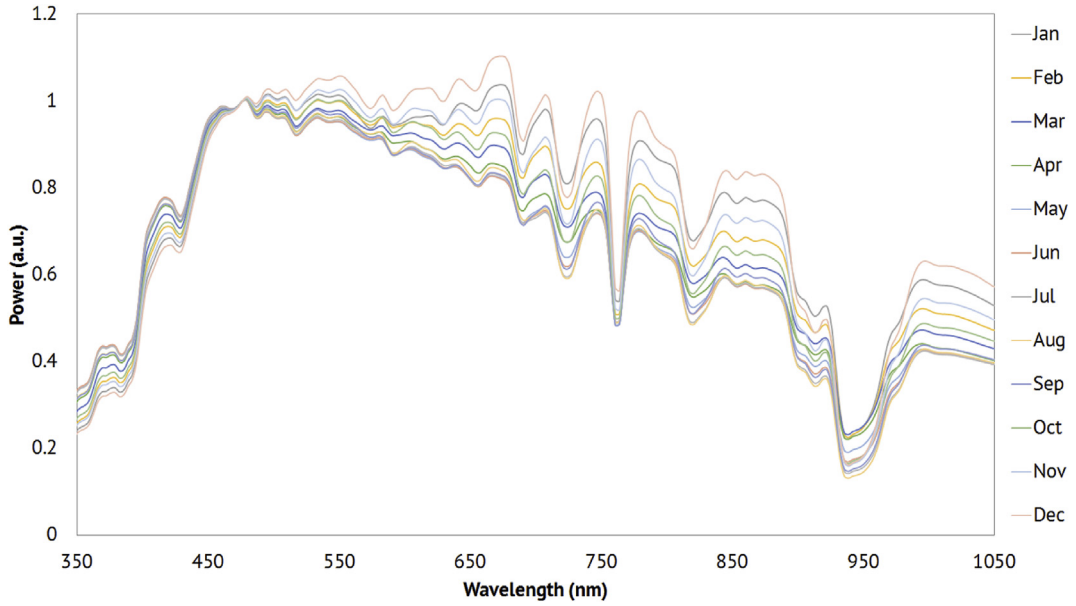

Fig. 2. Averaged, normalized solar spectra determined at 13:00 for all months of the year 2015 measured at Utrecht University.

with the performance of the cells under illumination by a standard solar spectrum. Under outdoor sunlight conditions, the spectrum that the PV cell sees is different and as a result the measured currents will also be different. So, the effect of a different spectrum on the PR can be estimated by calculating the difference in performance of a LSC under standard spectral conditions and under the actual solar spectrum. For this we define the mismatch factor (MM). For MM, the response of the cell to a specific wavelength must be known. This is called the spectral response of the cell, SR(λ). Here the spectral response of the combined cell and LSC plate must be used. The MM between the cell response under AM1.5 spectrum and under the actual solar spectrum at a given time can be derived using the following formula:

$$\boldsymbol{MM} = \frac{\int \boldsymbol{E}(\lambda)_{\boldsymbol{sun}}\, \boldsymbol{SR_{test}}(\lambda)\boldsymbol{d}\lambda * \int \boldsymbol{E}(\lambda)_{\boldsymbol{AM1.5}}\, \boldsymbol{SR_{ref}}(\lambda)\boldsymbol{d}\lambda}{\int \boldsymbol{E}(\lambda)_{\boldsymbol{sun}}\, \boldsymbol{SR_{ref}}(\lambda)\boldsymbol{d}\lambda * \int \boldsymbol{E}(\lambda)_{\boldsymbol{AM1.5}}\, \boldsymbol{SR_{test}}(\lambda)\boldsymbol{d}\lambda} \quad (2)$$

where $E(\lambda)_{sun}$ is the spectral irradiance of sun, $(\lambda)_{AM1.5}$ is the spectral irradiance of the AM1.5 reference spectrum, $SR(\lambda)_{test}$ is the SR of the test PV cell connected to the LSC, and $SR(\lambda)_{ref}$ is the SR of the reference PV cell as measured before it was connected.

As the current of a cell is given by:

$$I = \int E(\lambda)_{AM1.5}\, SR_{ref}(\lambda)\boldsymbol{d}\lambda \quad (3)$$

Equation (1) can be rewritten as:

$$MM = \frac{\int E(\lambda)_{sun}\, SR_{test}(\lambda)\boldsymbol{d}\lambda * I_{ref,AM1.5}}{\int E(\lambda)_{sun}\, SR_{ref}(\lambda)\boldsymbol{d}\lambda * \int E(\lambda)_{AM1.5}\, SR_{test}(\lambda)\boldsymbol{d}\lambda} \quad (4)$$

where $I_{ref,AM1.5}$ is the current of PV cell (or module) under AM1.5 spectral conditions as measured before connection to the LSC. The correct current $I_{test,AM1.5}$ can now be estimated from the measured current $I_{test,\ lamp}$ and the MM by

$$\boldsymbol{I_{test,sun}} = \boldsymbol{I_{test,AM1.5}}\ x\ MM \quad (5)$$

Monthly averaged spectral data as measured at the University of Utrecht were used together with a typical spectral response from one of the ECN c-Si reference PV cells. The spectral response of a Red305 containing luminescent concentrator plate was measured in a previous project using a similar plate material [10]. The shape of the SR is mainly determined by the absorption of the dye and the attached PV cell but the actual response numbers can differ due to variations in the connection between the plate and the cell. For this reason a scaling factor was used that was assumed to be constant over the year.

The result of this calculation is shown as the dotted line in Fig. 4 for the N/S oriented plate and in Fig. 5 for the E/W oriented one. It is clear that the fluctuations in the global trend of the PR can be nicely modeled. The position of the calculated results is arbitrary as it is determined by the scaling factor. The data reveals the dependence of cell strip positioning on the lightguide and differences in optical connections between the cell strips and the LSC plate. For the North/South orientation, the seasonal trend seems to be slightly different in the months June through August. This mismatch will be discussed later but appears to stem from increased cell heating.

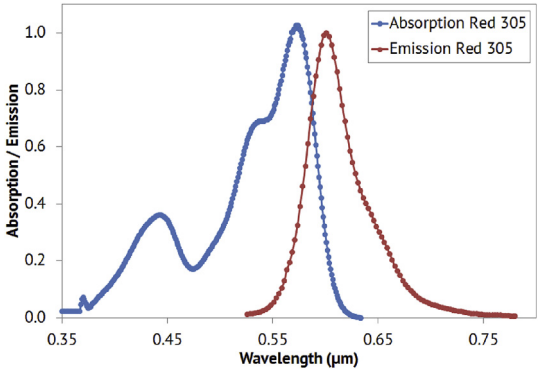

Fig. 3. Normalized absorption (blue line) and emission (red line) spectra of Red305 fluorescent dye embedded in PMMA. (For interpretation of the references to colour in this figure legend, the reader is referred to the web version of this article.)

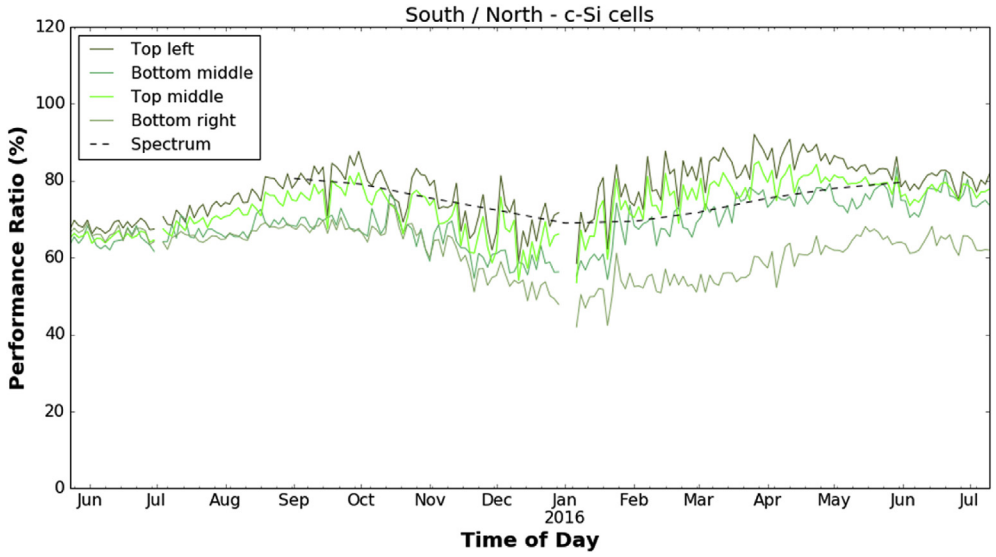

Fig. 4. Seasonal spectral changes compared to the PR of the North/South c-Si cells of the Red305 panel. The dotted line is the calculated PR based on the measured spectral changes.

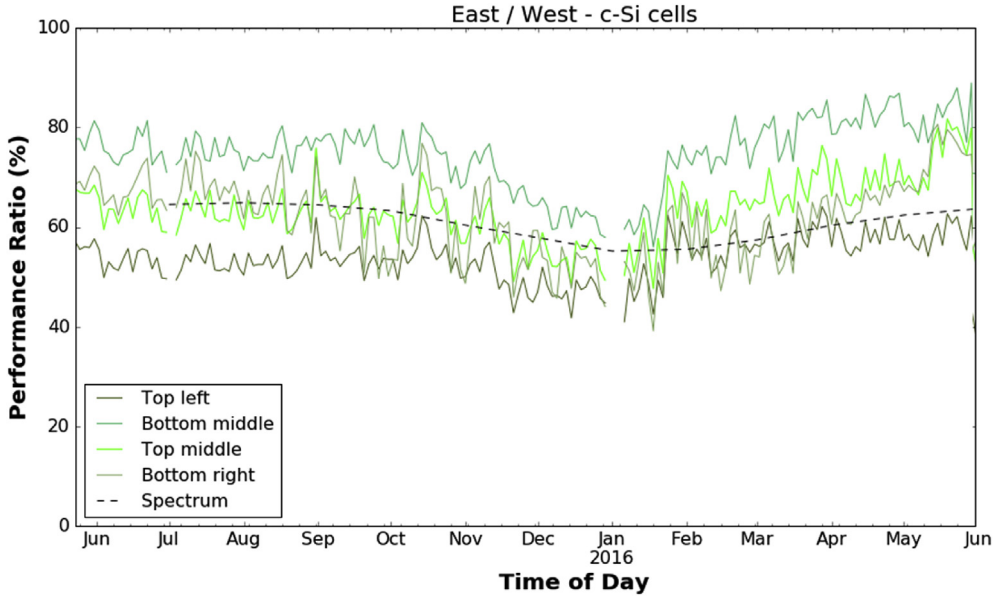

Fig. 5. Seasonal spectral changes compared to the PR of the East/West c-Si cells of the Red305panel. The dotted line is the calculated PR based on the measured spectral changes.

Table 1
Thermocouple labeling and positions on the solar noise barriers.

Thermocouple labels	Noise barrier, panel and cell position
T1	North/South noise barrier, Red305 LSC panel, TM c-Si cell
T2	North/South noise barrier, Red305 LSC panel, BM GaAs cell
T3	North/South noise barrier, Orange240 LSC panel, top c-Si cell
T4	North/South noise barrier, Orange240 LSC panel, bottom GaAs cell
T5	East/West noise barrier, Red305 LSC panel, TM c-Si cell
T6	East/West noise barrier, Red305 LSC panel, BM GaAs cell
T7	East/West noise barrier, Orange240 LSC panel, top c-Si cell
T8	East/West noise barrier, Orange240 LSC panel, bottom GaAs cell

3.2. Heat distribution within the LSC panel

To be able to measure the temperature of the cell strips on the LSC panels, we connected thermocouples to the back of 8 cell strips, on both orientations of panels and on both colored plates: the numbering and positioning of the thermocouples is shown in Table 1. We present data collected during a very sunny day (30 of June 2015) at 2-min intervals in Fig. 6, and hourly averaged temperatures in Fig. 7 for the whole field testing year.

The temperature data of the cells are given in terms of differences between the cell temperature and ambient temperature ($\Delta T = T_i - T_{ambient}$), which is the driving force of the heat transfer process. In other words, this temperature difference represents the difficulty of heat dissipation. The temperature difference ΔT of each cell is plotted against the total incident irradiation from both sides of the barrier (North + South, East + West). Measurement points that correspond to wind speed above 3 m/s were excluded because

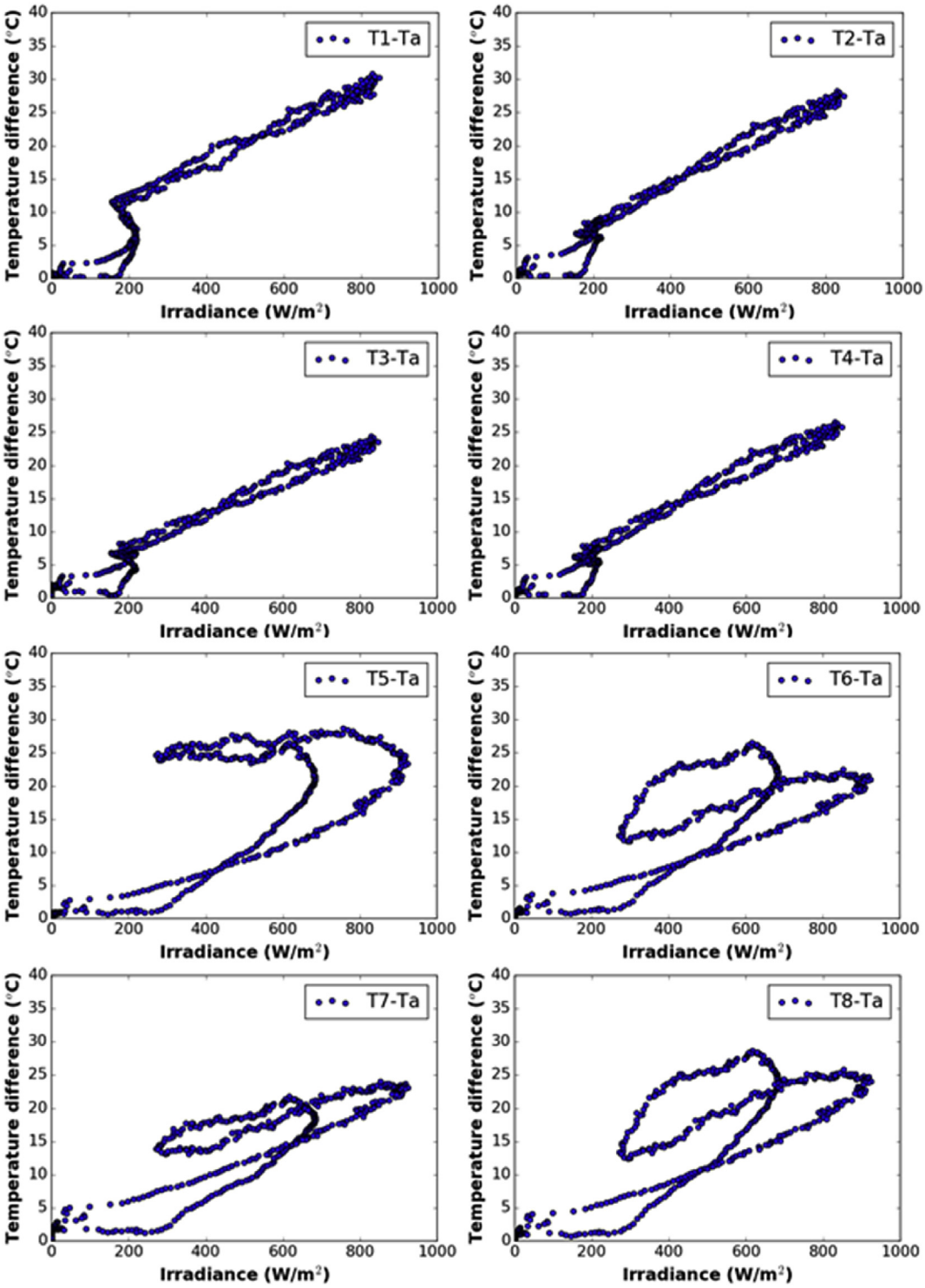

Fig. 6. Temperature distributions for a very sunny day of June 30, 2015. The identity of the individual thermocouples are described in Table 1. In summary, T1-T4 are facing North/South, T5-T8 face East/West. T1,3,5,7 are attached to the top of panels, T2,4,6,8 to the bottom of panels. T1,2,5,6 are attached the Red305 panels, and T3,4,7,8 are attached to Orange240 -panels.

there was too much scatter in the plots. The conduction and convection heat transfer to the cells tends to be linear for smaller wind speeds; higher wind speeds would affect the heat transfer mechanism.

Zooming out to the whole field testing year temperature data, the hourly ambient temperature data are presented in Fig. 7: the ambient temperatures are measured using a weather station mounted on top of the container housing the computers used to collect PV data.

In Fig. 8, the daily maximum cell temperatures for the year of field testing are displayed. In “blue” colors, the maximum temperatures of the cells of the North/South noise barrier are presented

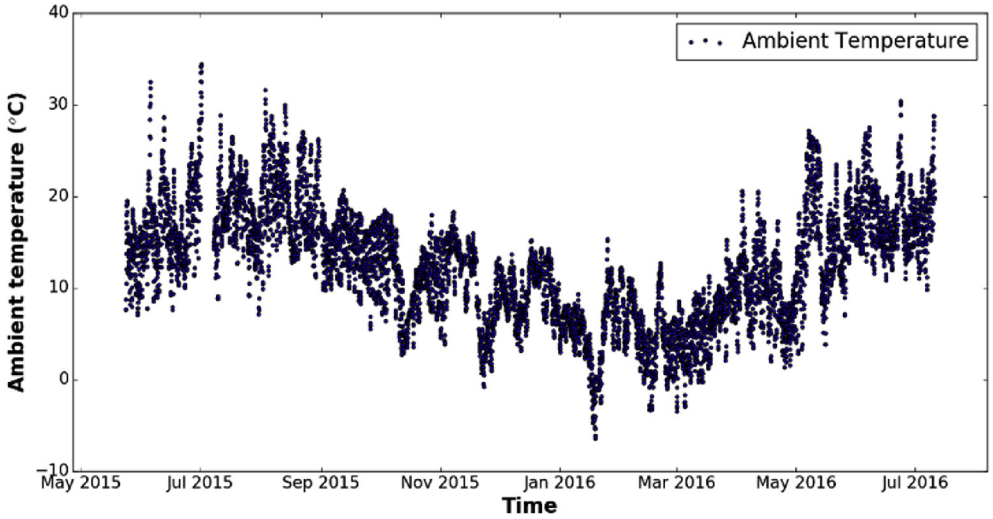

Fig. 7. Ambient temperatures of the field testing year at the measurement site.

while in "red" colors the ones of the East/West noise barrier. On average, it appears that the temperature for PV cells mounted to the North-South oriented LSCs suffer more from heating than the East/West oriented cells.

The highest cell temperatures were observed during the summer, and reached 60 °C while the ambient temperature was about 30 °C. In general, the cell temperatures of the North/South noise barriers appear to be higher by up to 5 °C compared to the same cells of the East/West barrier. A correlation between ΔT and incident irradiance for the whole field testing year appears in Fig. 9. The references to the cells are given in Table 1.

As can be seen in Fig. 4, there is a dip in performance during the winter months resulting from a shift in the effective solar spectrum reaching the panels, as one might expect. As described previously, PR calculations match the results of the measurements on the East/West oriented barrier (Fig. 5) but there is a mismatch during the summer (June through August) period for the North/South barriers (Fig. 6). The baseline powers for the panels were measured at room temperature before assembling the barriers. Normally, an increase of PV cell temperature results in a decrease in electrical performance [20–22]. The temperature of the cells during summer increases substantially, reducing the voltage of the cells and subsequent measured power output, but this is not included in calculations of the PR. The East/West PV cells show reduced temperature fluctuation, and hence the PR calculations appear a better match.

For the North/South noise barrier, the daily temperature difference is apparently directly dependent on the incident irradiance falling on the LSC panel: consider the first four graphs of Fig. 6. For the East/West noise barrier, the temperature dependence is not directly correlated to incident irradiance (second set of four graphs from Fig. 6). These daily trends are roughly mirrored in the yearly temperature data (see Fig. 9), in that the temperature differences for the North/South noise barrier appear to scale linearly with incident irradiance, while the East/West noise barrier again displays considerable variation in the temperature differences of the cells in comparison to the external temperatures.

One can speculate on some causes for the decreased temperature differences despite the higher intensity of incident light during

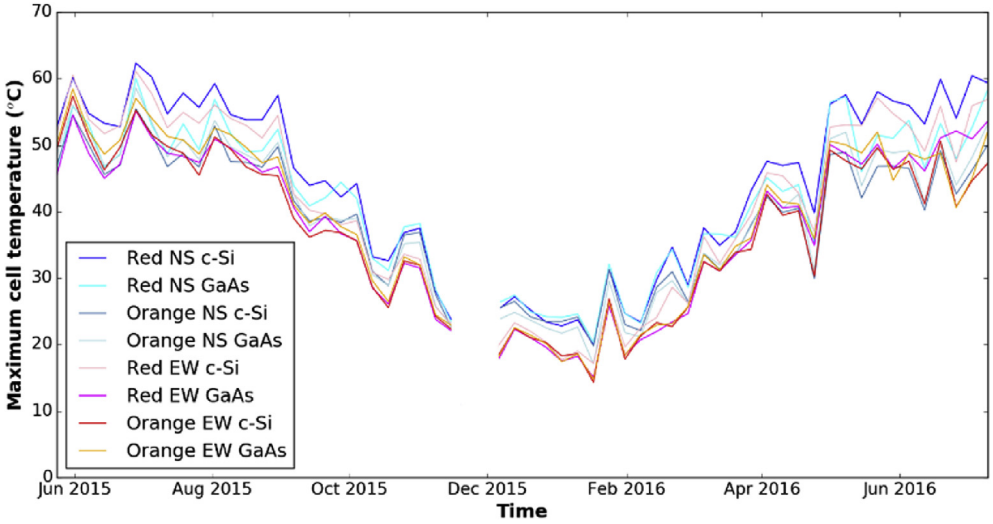

Fig. 8. Maximum daily cell temperatures throughout the year of field testing.

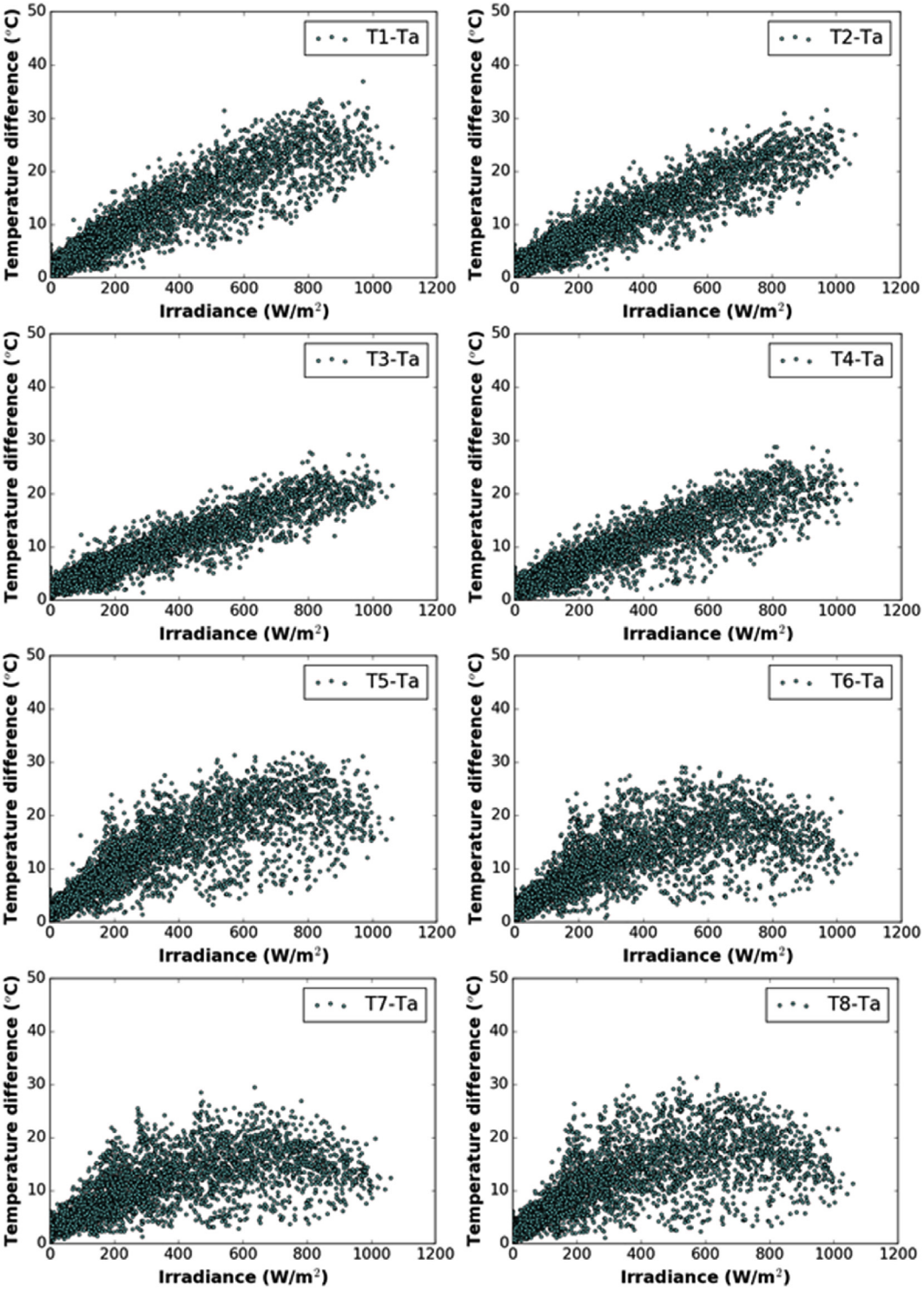

Fig. 9. Temperature distribution over the period of one year as a function of irradiance. In summary, T1-T4 are facing North/South, T5-T8 face East/West. T1,3,5,7 are attached to the top of panels, T2,4,6,8 to the bottom of panels. T1,2,5,6 are attached the Red305 panels, and T3,4,7,8 are attached to Orange240 panels.

the course of the day for the East/West panels. One possibility is that the solar disc will first rise from the rear side of the East/West barrier and pass overhead near the middle of the day. During this mid-day period with highest intensity, the sun will be at a steep incident angle with respect to the East/West panel, reducing the surface area for collecting the light as well as increased reflection of the IR light from the surface, allowing cell cooling. As the day advances, the somewhat less intense light becomes incident more normal to the barrier face, resulting in more direct illumination and system heating. This explanation is perhaps supported by the fact the North/South facing barrier is always situated as to be facing more directly to the solar disc during all times of the day, and thus would show a more regular pattern of illumination and heating. These variations in surface illumination are supported by the

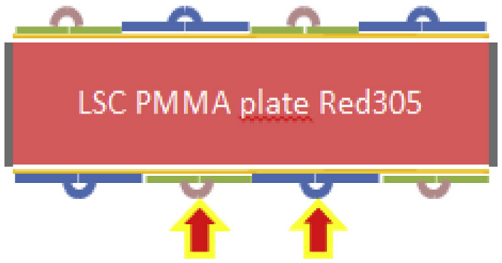

Fig. 10. Diagram indicating the cells monitored for effects of cloud cover. The green lines refer to the c-Si strip cells, and the blue lines to the GaAs strip cells. (For interpretation of the references to colour in this figure legend, the reader is referred to the web version of this article.)

electrical performance data as a function of solar motion seen in our previous work [13], and the data in Fig. 6, where for the East/West panel the oddly shaped, looped responses are likely due to the sun passing over the top of the device. This considerable fluctuation in cell temperature with irradiance suggests the barrier frame needs to be redesigned, perhaps by including a heat sink that it will better insulate and minimize cell temperature variation throughout the day. Still, the cells on the LSC function at slightly lower temperatures to directly illuminated cells [19], which will have a positive effect on the device performance.

3.3. Effect of clouds

To compare the effects of cloudy skies on the LSC panel performance, we will define the clearness index (k_t) as the ratio of the global horizontal irradiance to the corresponding extraterrestrial

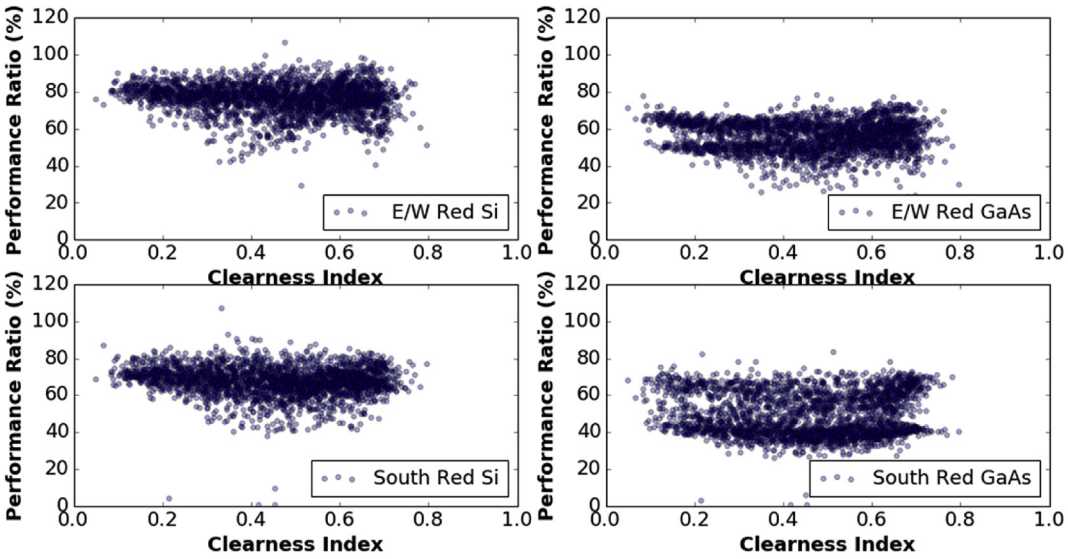

Fig. 11. The performance versus clearness index for four different cell strips on the Red305 LSC plates in both orientations.

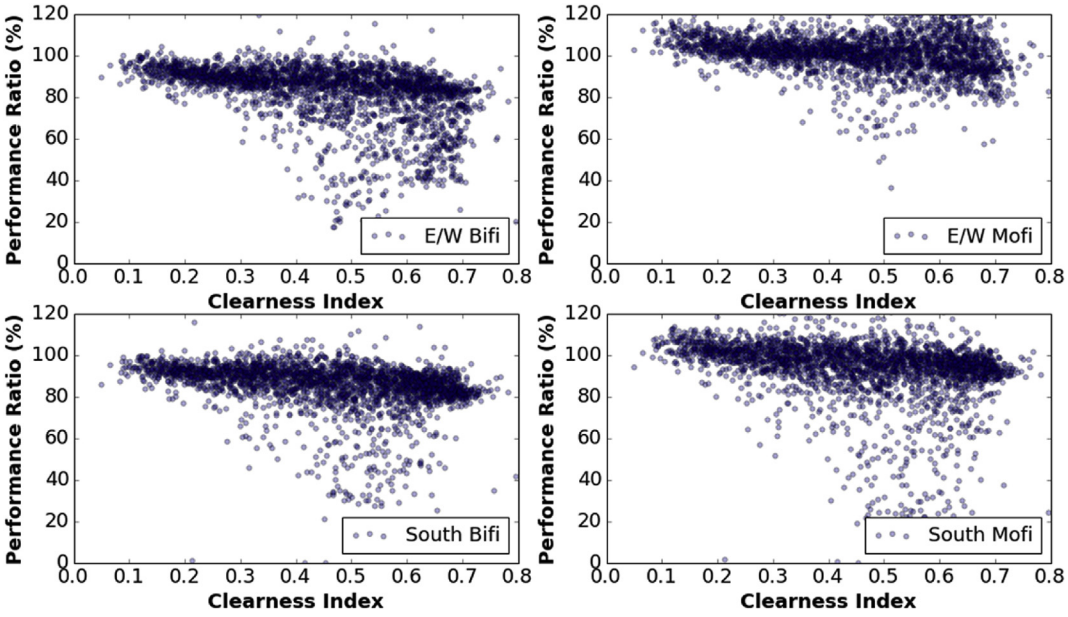

Fig. 12. The performance versus clearness index for the four different c-Si reference panels.

irradiance.

$$k_t = \frac{E_{GHI}}{E_{Extraterrestrial}} \quad (6)$$

The clearness index is an indication of cloud cover; for a completely cloudless sky, the clearness index is around 0.8. We report on the performance of the two cell strips indicated in Fig. 10. We have compared PR data of the Red305 LSC panels as a function of clearness index (Fig. 11) to both the bifacial (Bifi) and monofacial (Mofi) crystalline reference panels (Fig. 12) located immediately below the colored LSC panels (see Fig. 1b). The data of the Orange240 LSC panels was not analyzed because the photodegradation of the LSC plates has a greater influence on the performance than the clearness index.

Data was selected from between May 25, 2015 (start of the measurements) and Oct 1, 2015 to exclude any cross-shading of the North/South barrier by the East/West barrier. Note that we use DC performance ratios, because the panels and cells strips are not grid connected.

Clouds generally have an adverse effect on crystalline silicon PV panel performance [21]. The cloud cover can have a variety of compounding influences: the intensity, incoming direction of the incident irradiation and the spectral composition changes [22]. The effect of cloud cover on the LSC noise barrier panels is rather subtle. Fig. 11 shows the performance ratio plotted against the clearness index for four cell strips on the Red305 LSC plates in the East/West and in the North/South orientations. One could argue there is a slight increase in performance at low clearness, consistent with earlier results [9], and that in general the LSC responses are generally more independent of the cloud condition than the silicon-based cells of Fig. 12. Here we observe a slight decrease in performance ratio with increasing clearness index. This relation is most likely caused by heating up of the cells, decreasing their performance. Unfortunately, the actual temperature of the silicon cells is not available.

4. Conclusions

The performance of a full-size luminescent solar concentrator noise barrier has been monitored for over a year, and some basic insights have been gained into its functionality in both cloudy and sunny conditions, at various external temperatures, and over a range of solar positions. The data shows the barriers perform with as good or better efficiency in extremely cloudy conditions as under direct sunlight, partially a result of the improved spectral match of incident sunlight to the dye absorption spectra. The solar position appears to have a significant impact on the temperatures reached by attached photovoltaic cells, with the cells attached to the East/West barrier running significantly cooler to those attached to the North/South facing panel at the s' Hertogenbosch, Netherlands location. Collectively, this series of articles has provided insight into the functionality of large-scale LSC devices and provided many valuable tips to their manufacture, and given a number of indicators that must be considered and improved upon in the next generation design of the systems. It appears the performance of an LSC could be predicted for any location given detailed knowledge of the local solar conditions, which is a great step forward towards eventual commercialization of the devices.

Acknowledgements

The authors would like to acknowledge the SONOB project funded partially by the TKI ZEGO program. They would also like to thank Stijn Verkuilen, Eppo Zuur, Walter Groenewoud, and Peter Heijmans of Heijmans Wegen BV, Remco van der Heijden from Airbus DS, Alex Timmerman from Van Campen Industries, and Menno van den Donker from SEAC for many helpful discussions.

References

[1] M.G. Debije, P.P.C. Verbunt, Thirty years of luminescent solar concentrator research: solar energy for the built environment, Adv. Energy Mater. 2 (2012) 12–35.
[2] W.H. Weber, J. Lambe, Luminescent greenhouse collector for solar radiation, Appl. Opt. 15 (1976) 2299–2300.
[3] A. Goetzberger, W. Greubel, Solar energy conversion with fluorescent collectors, Appl. Phys. 14 (1977) 123–139.
[4] W.G.J.H.M. van Sark, K.W.J. Barnham, L.H. Slooff, A.J. Chatten, A. Büchtemann, A. Meyer, S.J. McCormack, R. Koole, D.J. Farrell, R. Bose, E.E. Bende, A.R. Burgers, T. Budel, J. Quilitz, M. Kennedy, T. Meyer, C. De M. Donega, A. Meijerink, D. Vanmaekelbergh, Luminescent Solar Concentrators – A review of recent results, Opt. Express 16 (2008) 21773–21792.
[5] S.M. Reda, Stability and photodegradation of phthalocyanines and hematoporphyrin doped PMMA as solar concentrators, Sol. Energy 81 (2007) 755–760.
[6] M.A. El-Shahawy, A.F. Mansour, Optical properties of some luminescent solar concentrators, J. Mater. Sci. Mater. Elect. 7 (1996) 171–174.
[7] A.F. Mansour, Outdoor testing of luminescent solar concentrators in a liquid polymer and bulk plate of PMMA, Polym. Test. 17 (1998) 153–162.
[8] S.M. El-Bashir, O.A. AlHarbi, M.S. AlSalhi, Thin-Film LSCs based on PMMA nanohybrid coatings: device optimization and outdoor performance, Int. J. Photoenergy (2013) 10.
[9] M.G. Debije, V.A. Rajkumar, Direct versus indirect illumination of a prototype luminescent solar concentrator, Sol. Energy 122 (2015) 334–340.
[10] L.H. Slooff, E.E. Bende, A.R. Burgers, T. Budel, M. Pravettoni, R.P. Kenny, E.D. Dunlop, A. Büchtemann, A luminescent solar concentrator with 7.1% power conversion efficiency, Phys. Status Solidi R 2 (2008) 257–259.
[11] J.C. Goldschmidt, M. Peters, A. Bösch, H. Helmers, F. Dimroth, S.W. Glunz, G.P. Willeke, Increasing the efficiency of fluorescent concentrator systems, Sol. Energy Mater. Sol. Cells 93 (2009) 176–182.
[12] L. Desmet, A.J.M. Ras, D.K.G. De Boer, M.G. Debije, Monocrystalline silicon photovoltaic luminescent solar concentrator with 4.2% power conversion efficiency, Opt. Lett. 37 (2012) 3087–3089.
[13] M. Kanellis, M.M. de Jong, L. Slooff, M.G. Debije, The solar noise barrier project: 1. Effect of incident light orientation on the performance of a large-scale luminescent solar concentrator noise barrier, Renew. Energy 103 (2016) 647–652.
[14] M.G. Debije, C. Tzikas, V.A. Rajkumar, M.M. de Jong, The solar noise barrier project: 2. The effect of street art on the performance of a large scale luminescent solar concentrator prototype, Renew. Energy 113 (2017) 1288–1292.
[15] G. Seybold, G. Wagenblast, New perylene and violanthrone dyestuffs for fluorescent collectors, Dyes Pigm. 11 (1989) 303–317.
[16] R. Gottschalg, D.G. Infield, M.J. Kearney, Experimental study of variations of the solar spectrum of relevance to thin film solar cells, Sol. Energy Mater. Sol. Cells 79 (2003) 527–537.
[17] V. Hisdal, Spectral distribution of global and diffuse solar radiation in Ny-Alesund, Spitsbergen, Polar Res. 5 (1987) 1–27.
[18] M. Donovan, B. Bourne, J. Roche, Efficiency VS. irradiance characterization of PV modules requires angle-of-incidence and spectral corrections, in: Photovoltaic Specialists Conference (PVSC), 35th IEEE, 2010, pp. 2301–2305.
[19] B. Herteleer, J. Cappelle, J. Driesen, Quantifying low-light behaviour of photovoltaic modules by identifying their irradiance-dependent efficiency from data sheets, in: 27th European Photovoltaic Solar Energy Conference, WIP, 2012, pp. 3714–3719.
[20] E. Skoplaki, J.A. Palyvos, On the temperature dependence of photovoltaic module electrical performance: a review of efficiency/power correlations, Sol. Energy 83 (2009) 614–624.
[21] S.R. Raga, F. Fabregat-Santiago, Temperature effects in dye-sensitized solar cells, Phys. Chem. Chem. Phys. 15 (2013) 2328–2336.
[22] D. Du, J. Darkwa, G. Kokogiannakis, Thermal management systems for Photovoltaics (PV) installations: a critical review, Sol. Energy 97 (2013) 238–254.